

A New Approach for Designing Well-Balanced Schemes for the Shallow Water Equations: A Combination of Conservative and Primitive Formulations

Remi Abgrall* and Yongle Liu†

Abstract

In this paper, we introduce a new approach for constructing robust well-balanced numerical methods for the one-dimensional Saint-Venant system with and without the Manning friction term. Following the idea presented in [R. Abgrall, Commun. Appl. Math. Comput. 5(2023), pp. 370-402], we first combine the conservative and non-conservative (primitive) formulations of the studied conservative hyperbolic system in a natural way. The solution is globally continuous and described by a combination of point values and average values. The point values and average values will then be evolved by two different forms of PDEs: a conservative version of the cell averages and a possibly non-conservative one for the points. We show how to deal with both the conservative and non-conservative forms of PDEs in a well-balanced manner. The developed schemes are capable of exactly preserving both the still-water and moving-water equilibria. Compared with existing well-balanced methods, this new class of scheme is nonlinear-equations-solver-free. This makes the developed schemes less computationally costly and easier to extend to other models. We demonstrate the behavior of the proposed new scheme on several challenging examples.

Key words: Shallow water equations, Well-balanced schemes, Steady states, Residual Distribution, MOOD paradigm.

AMS subject classification: 76M12, 65M08, 65M99, 35L65, 86-08

1 Introduction

The paper focus on the one-dimensional (1-D) Saint-Venant system of shallow water equations with non-flat bottom topography and Manning friction term, which is widely used to model the water flows in rivers, canals, lakes, reservoirs, and coastal areas. The studied system reads as

$$\begin{cases} h_t + q_x = 0, \\ q_t + \left(hu^2 + \frac{g}{2}h^2\right)_x = -ghZ_x - \frac{gn^2}{h^{\frac{7}{3}}}|q|q, \end{cases} \quad (1.1)$$

*Institute of Mathematics, University of Zürich, Winterthurerstrasse 190, CH 8057 Zürich, Switzerland; remi.abgrall@math.uzh.ch

†Institute of Mathematics, University of Zürich, Winterthurerstrasse 190, CH 8057 Zürich, Switzerland; liuy12017@mail.sustech.edu.cn

where g is the constant acceleration due to gravity, x is the spatial variable, and t is the time. $h(x, t)$ is the water depth, $u(x, t)$ is the velocity, and $q(x, t) := h(x, t)u(x, t)$ is the discharge. $Z(x)$ is the bottom elevation and n is the Manning coefficient.

The system (1.1) is a hyperbolic system of balance laws. Developing robust and accurate numerical methods for such a system is a challenging task as this nonlinear hyperbolic system admits both smooth and nonsmooth solutions. In addition, a good numerical scheme should be able to accurately respect a delicate balance between the flux and source term in (1.1). In particular, one is interested in developing well-balanced (WB) numerical schemes that are capable of exactly preserving (some of) steady states. If a stable but non-well-balanced scheme is used, then the numerical errors may trigger the appearance of artificial waves of magnitude larger than the size of the waves to be captured. In order to ameliorate this situation, one can do mesh refinement so that the numerical errors will be controlled by the truncation errors. However, such mesh refinement may be too computationally expensive or even unaffordable in practical applications. Therefore, one needs to develop WB schemes.

Steady states are of great practical importance since they minimize, if they are stable, the energy, and many physically relevant solutions of (1.1) are, in fact, small perturbations of these steady states. The smooth steady-state solutions of (1.1) satisfy the following time-independent system:

$$\begin{cases} q_x = 0, \\ (hu^2 + \frac{g}{2}h^2)_x = -ghZ_x - \frac{gn^2}{h^{7/3}}|q|q, \end{cases} \quad (1.2)$$

which can be integrated to obtain

$$q \equiv \hat{q} = \text{Const}, \quad E := \frac{u^2}{2} + g(h + Z) + Q \equiv \hat{E} = \text{Const}, \quad (1.3)$$

where

$$Q = \int_{\hat{x}}^x \frac{gn^2}{h^{4/3}}|u|u \, d\xi \quad (1.4)$$

is a global quantity with \hat{x} being an arbitrary number. In the case when $u \equiv 0$, the steady states (1.3) reduce to a particular class of steady states—still-water equilibria (“lake at rest”):

$$u \equiv 0, \quad w := h + Z \equiv \text{Const}, \quad (1.5)$$

where w is the water surface. In fact, still-water steady state (1.5) is a special case of the general moving-water steady state (1.3). If the bottom friction is neglected, that is, if $n = 0$, the general smooth moving-water equilibria are given by

$$q \equiv \hat{q} = \text{Const}, \quad E := \frac{u^2}{2} + g(h + Z) \equiv \hat{E} = \text{Const}. \quad (1.6)$$

In the past decades, many WB methods for the system (1.1) have been developed. Some of them are capable of preserving still-water steady states (1.5) only (see, e.g., [3, 5, 6, 20, 21, 24, 27, 28, 33, 34]), while others can preserve moving-water equilibria as well (see, e.g., [7, 9–12, 14, 17, 30, 32, 38]). One may notice that it is significantly more difficult to obtain WB schemes for moving-water equilibria, since a special way to recover the moving water equilibrium and a WB quadrature rule

of the source term is essential to design such schemes. The authors in [7, 9–12, 14, 17, 32, 37] first define a transformation between the conservative variables $(h, q)^\top$ and the equilibrium variables $(q, E)^\top$. Then, the polynomial reconstruction will be performed on the equilibrium variables and one can obtain the one-sided cell boundary point values of the equilibrium variables. Next, the one-sided cell boundary point values of the conservative variables can be recovered from the point values of the equilibrium variables. At this stage, one usually has to solve nonlinear equations, as it can be clearly seen from (1.3) or (1.6) that the transformation is nonlinear. Finally, WB evaluations of the numerical flux and approximation of the source term are computed using the obtained reconstructed point values of conservative variables. In order to recover the point values of conservative variables from the nonlinear transformation and reconstructed point values of equilibrium variables, a nontrivial root-finding mechanism should be carefully developed.

Very recently, the author in [1] proposed a new class of schemes that can combine several writings of the same hyperbolic problem and showed how to deal with both the conservative and non-conservative forms in a natural way. In these schemes, the solution is globally continuous and described by a combination of point values and average values. The author demonstrated that one can recover the conservation property from how the average is updated and has more flexibility to deal directly with the non-conservative form of the system. This new class of schemes is proved to satisfy a Lax-Wendroff-like theorem and also showed numerically that the convergence to the correct weak solution.

In this paper, inspired by the method introduced in [1], we develop a novel way of designing WB schemes. In addition to the conservative system (1.1), we simultaneously study the following non-conservative (primitive) formulation:

$$\begin{cases} h_t + hu_x + uh_x = 0, \\ u_t + uu_x + g(h + Z)_x = -\frac{gn^2}{h^{\frac{4}{3}}}|u|u. \end{cases} \quad (1.7)$$

Since we have more flexibility to enforce the WB property on the non-conservative form, unlike most of the existing works mentioned above, this new class of WB schemes does not require a nontrivial root-finding mechanism. More precisely, we design a WB finite-volume method for system (1.1) to evolve the cell averages of conservative variables $(h, q)^\top$ and simultaneously propose a WB residual distribution (RD) method for system (1.7) to evolve the point values of primitive variables $(h, u)^\top$. Given the average values of conservative variables and point values of primitive variables, we first compute the average and point values of equilibrium variables. Since now we have three degrees of freedom inside each cell, we then apply a third-order parabolic interpolant on these equilibrium variables and compute the related point values at the cell center. Next, we do the spatial discretizations on the equilibrium variables, which helps to ensure the WB property. It follows from (1.3) that the approximations of spatial derivatives appear in (1.7) can be obtained by solving some systems of linear equations. Unlike most of the existing methods, at this stage, we transform from the equilibrium variables to the primitive variables. Finally, we compute the fluctuation for system (1.7) and split the residual onto the nodes based on an upwind consideration. For numerically solving (1.1), we simply compute the numerical flux using the point values of primitive variables at the cell interfaces and a WB approximation of source term is given using the values of equilibrium variables. In addition to the WB property, the developed schemes are positivity-preserving. This attributes to the fact that we have applied the “draining time step” technique from [5, 6, 8, 17, 26] to the solver of (1.1) and a simply MOOD paradigm from [19, 36] equipped with a first-order scheme that has a Local Lax-Friedrichs’ flavour to the solver of (1.7).

The rest of the paper is organized as follows. In section 2, we introduce the new WB positive-preserving schemes for the conservative formulation (1.1) and the non-conservative formulation (1.7). In section 3, we present the numerical results, which demonstrate the WB property, positivity-preserving property, high resolution, and robustness of the proposed schemes. Finally, in section 4, we give some concluding remarks and comments on the future development and applications of the proposed WB schemes.

2 Schemes

In this section, we describe the third-order semi-discrete numerical schemes for the 1-D Saint-Venant system (1.1) and its non-conservative version (1.7). To this end, we first add an additional equation $Z_t = 0$ into (1.1) and rewrite it in a vector form as

$$\mathbf{U}_t + \mathbf{F}(\mathbf{U})_x = \mathbf{S}(\mathbf{U}), \quad \mathbf{U} = (h, q, Z)^\top, \quad (2.1)$$

where $\mathbf{U} \in \mathbb{R}^d$ and

$$\mathbf{F}(\mathbf{U}) = \begin{pmatrix} q \\ hu^2 + \frac{g}{2}h^2 \\ 0 \end{pmatrix}, \quad \mathbf{S}(\mathbf{U}) = \begin{pmatrix} 0 \\ -ghZ_x - Q_x \\ 0 \end{pmatrix}. \quad (2.2)$$

We also add an additional equation $Z_t = 0$ to (1.7) and rewrite it in the following vector form:

$$\mathbf{V}_t + J \frac{\partial \mathbf{V}}{\partial x} = \frac{\partial \mathbf{B}(\mathbf{V})}{\partial x}, \quad \mathbf{V} = (h, u, Z)^\top, \quad \mathbf{B} = (0, -Q, 0)^\top, \quad (2.3)$$

where $\mathbf{V} = \Psi(\mathbf{U})$, $\frac{\partial \mathbf{B}(\mathbf{V})}{\partial x} = (0, -Q_x, 0)^\top$, and J is the Jacobian matrix given by

$$J = \begin{pmatrix} u & h & 0 \\ g & u & g \\ 0 & 0 & 0 \end{pmatrix}. \quad (2.4)$$

We divide the computational domain into a set of uniform (for simplicity of presentation) cells $K_{j+\frac{1}{2}} := [x_j, x_{j+1}]$ of size $\Delta x = x_{j+1} - x_j$, which are centered at $x_{j+\frac{1}{2}} = (x_j + x_{j+1})/2$. We assume that at a certain time level t , the numerical solution of (2.1)–(2.2), realized in terms of its cell average $\bar{\mathbf{U}}_{j+\frac{1}{2}}(t) \approx \frac{1}{\Delta x} \int_{K_{j+\frac{1}{2}}} \mathbf{U}(x, t) dx$, is available. We denote the numerical solutions of (2.3)–(2.4) by $\mathbf{V}_j(t) \approx \mathbf{V}(x_j, t)$, which are also known at time t . Following the method introduced in [1], we evolve the cell averages $\bar{\mathbf{U}}_{j+\frac{1}{2}}$ in time by solving the following system of time-dependent ODEs:

$$\frac{d}{dt} \bar{\mathbf{U}}_{j+\frac{1}{2}} = -\frac{\mathcal{F}_{j+1} - \mathcal{F}_j}{\Delta x} + \bar{\mathbf{S}}_{j+\frac{1}{2}}, \quad (2.5)$$

where

$$\mathcal{F}_j = \mathbf{F}(\mathbf{U}_j) \stackrel{(2.2)}{=} \begin{pmatrix} q_j \\ h_j u_j^2 + \frac{g}{2} h_j^2 \\ 0 \end{pmatrix} \quad (2.6)$$

is a consistent numerical flux, which depends continuously of its arguments, and

$$\bar{\mathbf{S}}_{j+\frac{1}{2}} := \frac{1}{\Delta x} \int_{K_{j+\frac{1}{2}}} \mathbf{S}(\mathbf{U}(x, t)) dx \quad (2.7)$$

is an approximation of the cell average of source term. At the same time, the point values \mathbf{V}_j are also evolved by solving a system of time-dependent ODEs given by

$$\frac{d}{dt} \mathbf{V}_j = -(\overleftarrow{\Phi}_{j+\frac{1}{2}} \mathbf{V}_{j+\frac{1}{2}} + \overrightarrow{\Phi}_{j-\frac{1}{2}} \mathbf{V}_{j-\frac{1}{2}}), \quad (2.8)$$

where $\overleftarrow{\Phi}_{j+\frac{1}{2}} \mathbf{V}_{j+\frac{1}{2}} + \overrightarrow{\Phi}_{j-\frac{1}{2}} \mathbf{V}_{j-\frac{1}{2}}$ is a consistent approximation of $J \frac{\partial \mathbf{V}}{\partial x}(x_j) - \frac{\partial \mathbf{B}(\mathbf{V})}{\partial x}(x_j)$. Notice that all of the indexed quantities in (2.5)–(2.7), and (2.8) are time-dependent, but from here on, we omit this dependence for the sake of brevity.

As it was done in [1], we use the following discretization, which has an upwind flavour, to define $\overleftarrow{\Phi}_{j+\frac{1}{2}} \mathbf{V}_{j+\frac{1}{2}}$ and $\overrightarrow{\Phi}_{j-\frac{1}{2}} \mathbf{V}_{j-\frac{1}{2}}$:

$$\begin{aligned} \overleftarrow{\Phi}_{j+\frac{1}{2}} \mathbf{V}_{j+\frac{1}{2}} &= (J(\mathbf{V}_j))^- \delta_j^- \mathbf{V} - (\tilde{J}(\mathbf{V}_j))^- \delta_j^- \mathbf{B}, \\ \overrightarrow{\Phi}_{j-\frac{1}{2}} \mathbf{V}_{j-\frac{1}{2}} &= (J(\mathbf{V}_j))^+ \delta_j^+ \mathbf{V} - (\tilde{J}(\mathbf{V}_j))^+ \delta_j^+ \mathbf{B}, \end{aligned} \quad (2.9)$$

where $\delta_j^\pm \mathbf{V}$ and $\delta_j^\pm \mathbf{B}$ are the left-/right-biased finite difference (FD) approximations of $\frac{\partial \mathbf{V}}{\partial x}(x_j)$ and $\frac{\partial \mathbf{B}(\mathbf{V})}{\partial x}(x_j)$, respectively. Details on the computations of $\delta_j^\pm \mathbf{V}$ and $\delta_j^\pm \mathbf{B}$ are provided in §2.1. The one-sided values $(J(\mathbf{V}_j))^\pm$ and $(\tilde{J}(\mathbf{V}_j))^\pm$ are defined as

$$J(\mathbf{V}_j)^\pm = \Upsilon_j \begin{pmatrix} \lambda_1^\pm & 0 & 0 \\ 0 & \lambda_2^\pm & 0 \\ 0 & 0 & \lambda_3^\pm \end{pmatrix} \Upsilon_j^{-1} := \Upsilon_j \Lambda^\pm \Upsilon_j^{-1} \quad (2.10)$$

and

$$\tilde{J}(\mathbf{V}_j)^\pm = \Upsilon_j \begin{pmatrix} \frac{\lambda_1^\pm}{\lambda_1} & 0 & 0 \\ 0 & \frac{\lambda_2^\pm}{\lambda_2} & 0 \\ 0 & 0 & \frac{\lambda_3^\pm}{\lambda_3} \end{pmatrix} \Upsilon_j^{-1} := \Upsilon_j \tilde{\Lambda}^\pm \Upsilon_j^{-1}. \quad (2.11)$$

Here, $\lambda_1 = 0$, $\lambda_2 = u_j - \sqrt{gh_j}$, and $\lambda_3 = u_j + \sqrt{gh_j}$ are the three eigenvalues of Jacobian J in (2.4). $\Upsilon_j = \Upsilon(\mathbf{V}_j)$ is the corresponding eigenvector matrix given by

$$\Upsilon_j = \begin{pmatrix} -\frac{gh_j}{c_j} & -\sqrt{\frac{h_j}{g}} & \sqrt{\frac{h_j}{g}} \\ \frac{gu_j}{c_j} & 1 & 1 \\ 1 & 0 & 0 \end{pmatrix} \quad (2.12)$$

with $c_j = gh_j - u_j^2$. When $u_j = \pm \sqrt{gh_j}$, we simply take $\overleftarrow{\Phi}_{j+\frac{1}{2}} \mathbf{V}_{j+\frac{1}{2}} = \overrightarrow{\Phi}_{j-\frac{1}{2}} \mathbf{V}_{j-\frac{1}{2}} = 0$.

2.1 Well-balanced Approximations

In order to complete the computation in (2.9), one needs to compute the FD approximations $\delta_j^\pm \mathbf{V}$ and $\delta_j^\pm \mathbf{B}$, which depend on some \mathbf{V}_j and $\mathbf{V}_{j+\frac{1}{2}} \approx \mathbf{V}(x_{j+\frac{1}{2}})$. Given the point value \mathbf{U}_j and the cell average $\overline{\mathbf{U}}_{j+\frac{1}{2}}$, we first construct a third-order parabolic interpolant of \mathbf{U} defined on $K_{j+\frac{1}{2}}$

$$\tilde{\mathbf{U}}(x) = \mathbf{U}_j \ell_0(\xi) + \overline{\mathbf{U}}_{j+\frac{1}{2}} \ell_{\frac{1}{2}}(\xi) + \mathbf{U}_{j+1} \ell_1(\xi), \quad \xi = \frac{x - x_j}{\Delta x} \in [0, 1], \quad (2.13)$$

where $\mathbf{U}_j = \Psi(\mathbf{V}_j)$ for all j and

$$\ell_0(\xi) = (1 - \xi)(1 - 3\xi), \quad \ell_1(\xi) = \xi(3\xi - 2), \quad \ell_{\frac{1}{2}}(\xi) = 6\xi(1 - \xi).$$

Then, we compute the point values $\mathbf{U}_{j+\frac{1}{2}} := \tilde{\mathbf{U}}(x_{j+\frac{1}{2}}) = \frac{3}{2} \overline{\mathbf{U}}_{j+\frac{1}{2}} - \frac{1}{4}(\mathbf{U}_j + \mathbf{U}_{j+1})$ for all j , which gives

$$\mathbf{V}_{j+\frac{1}{2}} = \Psi^{-1}(\mathbf{U}_{j+\frac{1}{2}}). \quad (2.14)$$

Next, we rewrite the global quantity Q defined in (1.4) in a recursive way and then approximate the yield integration part by the Simpson's rule. Namely, we take

$$\begin{aligned} Q_{j+1} &= Q_j + \int_{x_j}^{x_{j+1}} \frac{gn^2}{h^{\frac{4}{3}}} |u| u \, dx \\ &\approx Q_j + \frac{gn^2 \Delta x}{6} \left(\frac{|u_j| u_j}{(h_j)^{4/3}} + \frac{|u_{j+1}| u_{j+1}}{(h_{j+1})^{4/3}} + 4 \frac{|u_{j+\frac{1}{2}}| u_{j+\frac{1}{2}}}{(h_{j+\frac{1}{2}})^{4/3}} \right), \end{aligned} \quad (2.15)$$

where $u_{j+\frac{1}{2}} := q_{j+\frac{1}{2}}/h_{j+\frac{1}{2}}$ and $Q_1 = 0$ as we simply take $\hat{x} = x_1$ in (1.4). At the same time, we set $Q_{j+\frac{1}{2}} := \frac{1}{2}(Q_j + Q_{j+1})$. Finally, one can use these obtained point values and the discretizations provided in [1, §3] to compute $\delta_j^\pm \mathbf{V}$ and $\delta_j^\pm \mathbf{B}$. However, it is easy to show that the resulting scheme can only preserve the simple ‘‘lake at rest’’ steady state (1.5). In order to preserve a wider class of complicate equilibria, such as (1.3) and (1.6), it is quite well-known that one has to perform the construction on the equilibrium variables; see, e.g., [11, 12, 15, 16, 27, 37]. We therefore turn to construct the equilibrium variables $\mathbf{E} = (q, E)^\top$ and proceed as follows.

First, we compute the point values $\mathbf{E}_j = (q_j, E_j)^\top$ and $\overline{\mathbf{E}}_{j+\frac{1}{2}} = (\overline{q}_{j+\frac{1}{2}}, \overline{E}_{j+\frac{1}{2}})^\top$ for all j as follows:

$$\begin{aligned} q_j &:= h_j u_j, \quad E_j = \frac{u_j^2}{2} + g(h_j + Z_j) + Q_j, \\ \overline{E}_{j+\frac{1}{2}} &= \frac{\overline{u}_{j+\frac{1}{2}}^2}{2} + g(\overline{h}_{j+\frac{1}{2}} + \overline{Z}_{j+\frac{1}{2}}) + Q_{j+\frac{1}{2}}, \end{aligned} \quad (2.16)$$

where $\overline{u}_{j+\frac{1}{2}} := \overline{q}_{j+\frac{1}{2}}/\overline{h}_{j+\frac{1}{2}}$. We then apply the third-order parabolic interpolant in (2.13) on \mathbf{E} to obtain

$$\mathbf{E}_{j+\frac{1}{2}} = \frac{3}{2} \overline{\mathbf{E}}_{j+\frac{1}{2}} - \frac{1}{4}(\mathbf{E}_j + \mathbf{E}_{j+1}). \quad (2.17)$$

Then, a third-order parabolic polynomial approximation of \mathbf{E} is constructed as

$$R_{\mathbf{E}}(x) = \mathbf{E}_j L_0(\xi) + \mathbf{E}_{j+\frac{1}{2}} L_{\frac{1}{2}}(\xi) + \mathbf{E}_{j+1} L_1(\xi), \quad (2.18)$$

where $\xi = \frac{x-x_j}{\Delta x} \in [0, 1]$ for $x \in K_{j+\frac{1}{2}}$ and

$$L_0(\xi) = (1 - \xi)(1 - 2\xi), \quad L_1(\xi) = \xi(2\xi - 1), \quad L_{\frac{1}{2}}(\xi) = 4\xi(1 - \xi). \quad (2.19)$$

Similarly, a third-order parabolic approximation of Z reads as

$$R_Z(x) = Z_j L_0(\xi) + Z_{j+\frac{1}{2}} L_{\frac{1}{2}}(\xi) + Z_{j+1} L_1(\xi). \quad (2.20)$$

Consequently, we can calculate the FD approximations of $\delta_j^\pm \mathbf{E} = (\delta_j^\pm q, \delta_j^\pm E)^\top$ and $\delta_j^\pm Z$ using the discretization provided in [1, §3]:

$$\begin{aligned} \delta_j^+ \mathbf{E} &= \frac{1}{\Delta x} (\mathbf{E}_{j-1} - 4\mathbf{E}_{j-\frac{1}{2}} + 3\mathbf{E}_j), & \delta_j^- \mathbf{E} &= \frac{1}{\Delta x} (-3\mathbf{E}_j + 4\mathbf{E}_{j+\frac{1}{2}} - \mathbf{E}_{j+1}), \\ \delta_j^+ Z &= \frac{1}{\Delta x} (Z_{j-1} - 4Z_{j-\frac{1}{2}} + 3Z_j), & \delta_j^- Z &= \frac{1}{\Delta x} (-3Z_j + 4Z_{j+\frac{1}{2}} - Z_{j+1}), \end{aligned} \quad (2.21)$$

which are second-order accuracy and can be obtained by taking derivative of (2.18) and (2.20), respectively.

Next, the left- and right-biased FD approximations of $\delta_j^\pm h$ and $\delta_j^\pm u$ are obtained by solving the following linear system of equations at $x = x_j$, which arises from the definition of the equilibrium variable in (1.3):

$$\begin{cases} u_j(\delta_j^\pm h) + h_j(\delta_j^\pm u) = \delta_j^\pm q, \\ g(\delta_j^\pm h) + u_j(\delta_j^\pm u) = \delta_j^\pm E - g\delta_j^\pm Z - \delta_j^\pm Q, \end{cases} \quad (2.22)$$

where

$$\delta_j^+ Q = \frac{1}{\Delta x} (Q_{j-1} - 4Q_{j-\frac{1}{2}} + 3Q_j), \quad \delta_j^- Q = \frac{1}{\Delta x} (-3Q_j + 4Q_{j+\frac{1}{2}} - Q_{j+1}).$$

Finally, we describe a WB discretization of $\bar{\mathbf{S}}_j$ such that the general steady states (1.3) will be preserved by the schemes (2.5) and (2.7). In fact, since $S^{(1)} \equiv 0$, we only need to design a WB approximation of the second component:

$$\bar{S}_{j+\frac{1}{2}}^{(2)} \approx \frac{1}{\Delta x} \int_{K_{j+\frac{1}{2}}} S^{(2)} dx = \frac{1}{\Delta x} \int_{K_{j+\frac{1}{2}}} (-ghZ_x - Q_x) dx. \quad (2.23)$$

Note that using the definition of equilibrium variable E , $S^{(2)}$ in (2.23) can be expressed as

$$S^{(2)} = (hu^2)_x + \frac{g}{2}(h^2)_x - uq_x - hE_x, \quad (2.24)$$

which is then substituted into (2.23) and yields

$$\begin{aligned} \bar{S}_{j+\frac{1}{2}}^{(2)} &\approx \frac{1}{\Delta x} \int_{K_{j+\frac{1}{2}}} \left[(hu^2)_x + \frac{g}{2}(h^2)_x - uq_x - hE_x \right] dx \\ &= \frac{1}{\Delta x} \left[h_{j+1}u_{j+1}^2 - h_ju_j^2 + \frac{g}{2}(h_{j+1}^2 - h_j^2) \right] - \frac{1}{\Delta x} \int_{K_{j+\frac{1}{2}}} (uq_x + hE_x) dx. \end{aligned} \quad (2.25)$$

In the end, we use the Simpson's rule to approximate the integral in the second line in (2.25) and end up with

$$\begin{aligned} \bar{S}_{j+\frac{1}{2}}^{(2)} &\approx \frac{1}{\Delta x} \left[h_{j+1} u_{j+1}^2 - h_j u_j^2 + \frac{g}{2} (h_{j+1}^2 - h_j^2) \right] \\ &\quad - \frac{1}{6} \left[u_j(q_x)_j + u_{j+1}(q_x)_{j+1} + 4u_{j+\frac{1}{2}}(q_x)_{j+\frac{1}{2}} \right] \\ &\quad - \frac{1}{6} \left[h_j(E_x)_j + h_{j+1}(E_x)_{j+1} + 4h_{j+\frac{1}{2}}(E_x)_{j+\frac{1}{2}} \right], \end{aligned} \quad (2.26)$$

where

$$\begin{aligned} (\mathbf{E}_x)_j &= \frac{1}{\Delta x} (-3\mathbf{E}_j + 4\mathbf{E}_{j+\frac{1}{2}} - \mathbf{E}_{j+1}), \\ (\mathbf{E}_x)_{j+1} &= \frac{1}{\Delta x} (\mathbf{E}_j - 4\mathbf{E}_{j+\frac{1}{2}} + 3\mathbf{E}_{j+1}), \\ (\mathbf{E}_x)_{j+\frac{1}{2}} &= \frac{1}{\Delta x} (-\mathbf{E}_j + \mathbf{E}_{j+1}) \end{aligned}$$

for $\mathbf{E} = (q, E)^\top$.

Remark 2.1 *In order to guarantee the WB property of the developed schemes, we use (2.22) to compute the WB FD approximations of $\delta_j^\pm h$ and $\delta_j^\pm u$. However, when the numerical solution is away from the steady state, we prefer directly using the reconstruction on the variable \mathbf{V} to compute the corresponding FD approximations, rather than (2.22). Namely, when $\Gamma_{j+\frac{1}{2}} > \tau$, we take*

$$\delta_j^+ h = \frac{1}{\Delta x} (h_{j-1} - 4h_{j-\frac{1}{2}} + 3h_j), \quad \delta_j^+ u = \frac{1}{\Delta x} (u_{j-1} - 4u_{j-\frac{1}{2}} + 3u_j)$$

and similarly when $\Gamma_{j-\frac{1}{2}} > \tau$, we take

$$\delta_j^- h = \frac{1}{\Delta x} (-3h_j + 4h_{j+\frac{1}{2}} - h_{j+1}), \quad \delta_j^- u = \frac{1}{\Delta x} (-3u_j + 4u_{j+\frac{1}{2}} - u_{j+1}).$$

Here $\Gamma_{j+\frac{1}{2}} \in [0, 1]$ is a parameter that depends on the quantity $|E_j - E_{j+1}|$. When the difference between \hat{E}_j and E_{j+1} is small enough, $\Gamma_{j+\frac{1}{2}}$ tends to 0, otherwise it is close to 1. We will define this parameter in section 2.2. τ is a small threshold value and in all of the numerical experiments reported in section 3, we take $\tau = 10^{-3}$.

Remark 2.2 *We would like to point out that once the point values $\{h_{j+\frac{1}{2}}, q_{j+\frac{1}{2}}\}$ are obtained, then we can obtain the point values $u_{j+\frac{1}{2}} = q_{j+\frac{1}{2}}/h_{j+\frac{1}{2}}$, which is needed in the computations of (2.15) and (2.26). However, this computation has to be desingularized to avoid division by either zero or a very small number. We take a small number $\varepsilon = 10^{-6}$ and use the following desingularization technique to compute*

$$u_{j+\frac{1}{2}} = \begin{cases} \frac{q_{j+\frac{1}{2}}}{h_{j+\frac{1}{2}}} & \text{if } h_{j+\frac{1}{2}} > \varepsilon, \\ \frac{\sqrt{2}q_{j+\frac{1}{2}}h_{j+\frac{1}{2}}}{\sqrt{h_{j+\frac{1}{2}}^4 + \max(h_{j+\frac{1}{2}}^4, \varepsilon^4)}} & \text{otherwise.} \end{cases} \quad (2.27)$$

For consistency, we then use (2.27) to recompute the point values $q_{j+\frac{1}{2}} = h_{j+\frac{1}{2}} u_{j+\frac{1}{2}}$. Furthermore, one can notice that the same problem may occur in the computation of $\bar{u}_{j+\frac{1}{2}}$ if the cell averages

$\bar{h}_{j+\frac{1}{2}}$ become very small or zero. Therefore, we adopt the same desingularization technique to adjust the computation.

We now prove that the numerical schemes given by (2.5), (2.26), and (2.8) are WB in the sense that the following two theorems hold.

Theorem 2.3 (Well-Balanced for Still-Water) *If the discrete data are at a steady state (1.5), namely, the discrete data satisfy the following relations:*

$$u_j = u_{j+\frac{1}{2}} \equiv 0, \quad w_j = h_j + Z_j = w_{j+\frac{1}{2}} = h_{j+\frac{1}{2}} + Z_{j+\frac{1}{2}} \equiv \widehat{w} = \text{Const}, \quad \forall j, \quad (2.28)$$

then, the proposed schemes given by (2.5), (2.26), and (2.8) are WB. Namely,

$$\frac{d}{dt} \bar{\mathbf{U}}_{j+\frac{1}{2}} = \mathbf{0} \quad \text{and} \quad \frac{d}{dt} \mathbf{V}_j = \mathbf{0}. \quad (2.29)$$

Proof. In order to prove this theorem, we need to show that the right-hand sides of (2.5) and (2.8) vanish as long as the data satisfy (2.28).

First, since $u_j \equiv 0$ for all j , it is easy to obtain

$$\mathcal{F}_{j+1}^{(1)} = h_{j+1}u_{j+1} \equiv 0 \quad \text{and} \quad \mathcal{F}_j^{(1)} = h_j u_j \equiv 0. \quad (2.30)$$

Simultaneously, we can compute the second component of the numerical fluxes, which reads as

$$\mathcal{F}_{j+1}^{(2)} = \frac{g}{2} h_{j+1}^2 \quad \text{and} \quad \mathcal{F}_j^{(2)} = \frac{g}{2} h_j^2. \quad (2.31)$$

We then note that $q_j = q_{j+\frac{1}{2}} = 0$, $E_j = gw_j \equiv g\widehat{w}$ and $E_{j+\frac{1}{2}} = gw_{j+\frac{1}{2}} \equiv g\widehat{w}$ for all j when the solution satisfies the discrete steady state (2.28). Hence, (2.26) reduces to

$$\bar{\mathcal{S}}_{j+\frac{1}{2}}^{(2)} = \frac{g}{2\Delta x} (h_{j+1}^2 - h_j^2). \quad (2.32)$$

Next, we use (2.30), (2.31), and (2.32) to verify that the right-hand side of (2.5) vanishes, namely, $\frac{d}{dt} \bar{\mathbf{U}}_{j+\frac{1}{2}} = \mathbf{0}$.

We proceed with proving that the right-hand side of (2.8) vanishes. To this end, we first solve (2.22) to obtain

$$\delta_j^\pm h = \delta_j^\pm w - \delta_j^\pm Z \quad \text{and} \quad \delta_j^\pm u \equiv 0.$$

Here, we have used the fact that $\frac{1}{g}\delta_j^\pm E = \delta_j^\pm w$ and $\delta_j^\pm Q = 0$ at the steady state (2.28). We then use the formulae given by (2.10) and (2.12) to compute

$$J(\mathbf{V}_j)^\pm = \begin{pmatrix} \pm \frac{\sqrt{gh_j}}{2} & \frac{h_j}{2} & \pm \frac{\sqrt{gh_j}}{2} \\ \frac{g}{2} & \pm \frac{\sqrt{gh_j}}{2} & \frac{g}{2} \\ 0 & 0 & 0 \end{pmatrix},$$

which can be substituted into (2.9) to obtain

$$\overleftarrow{\Phi}_{j+\frac{1}{2}} \mathbf{V}_{j+\frac{1}{2}} = \begin{pmatrix} -\frac{\sqrt{gh_j}}{2} \delta_j^- w \\ -\frac{g}{2} \delta_j^- w \\ 0 \end{pmatrix} \quad \text{and} \quad \overrightarrow{\Phi}_{j-\frac{1}{2}} \mathbf{V}_{j-\frac{1}{2}} = \begin{pmatrix} \frac{\sqrt{gh_j}}{2} \delta_j^+ w \\ \frac{g}{2} \delta_j^+ w \\ 0 \end{pmatrix}.$$

Since $w_j = w_{j+\frac{1}{2}}$ for all j , it is easy to induce that $\delta_j^\pm w = 0$ from (2.21), and thus

$$\overleftarrow{\Phi}_{j+\frac{1}{2}} \mathbf{v}_{j+\frac{1}{2}} = \overrightarrow{\Phi}_{j-\frac{1}{2}} \mathbf{v}_{j-\frac{1}{2}} = \mathbf{0},$$

which implies that $\frac{d}{dt} \mathbf{V}_j = \mathbf{0}$. This completes the proof of the theorem. \blacksquare

Theorem 2.4 (Well-Balanced for Moving-Water) *If the discrete data are at a steady state (1.3), namely, the discrete data satisfy the following relations:*

$$q_j = q_{j+\frac{1}{2}} \equiv \widehat{q} = \text{Const}, \quad E_j = E_{j+\frac{1}{2}} \equiv \widehat{E} = \text{Const}, \quad \forall j, \quad (2.33)$$

then, the proposed schemes given by (2.5), (2.26), and (2.8) are WB. That is, (2.29) also holds here.

Proof. On one hand, we note that in all of the considered cells, $(q_x)_j = (q_x)_{j+\frac{1}{2}} \equiv 0$ and $(E_x)_j = (E_x)_{j+\frac{1}{2}} \equiv 0$, and hence (2.26) reduces to

$$\overline{S}_{j+\frac{1}{2}}^{(2)} = \frac{1}{\Delta x} \left[h_{j+1} u_{j+1}^2 - h_j u_j^2 + \frac{g}{2} (h_{j+1}^2 - h_j^2) \right]. \quad (2.34)$$

We then compute the right-hand sides of (2.5) in a component-wise manner:

$$\begin{aligned} \frac{d}{dt} \overline{U}_j^{(1)} &= -\frac{\mathcal{F}_{j+1}^{(1)} - \mathcal{F}_j^{(1)}}{\Delta x} = -\frac{q_{j+1} - q_j}{\Delta x} \stackrel{(2.33)}{=} 0, \\ \frac{d}{dt} \overline{U}_j^{(2)} &= -\frac{\mathcal{F}_{j+1}^{(2)} - \mathcal{F}_j^{(2)}}{\Delta x} = -\frac{h_{j+1} u_{j+1}^2 - h_j u_j^2 + \frac{g}{2} (h_{j+1}^2 - h_j^2)}{\Delta x} + \overline{S}_{j+\frac{1}{2}}^{(2)} \stackrel{(2.34)}{=} 0, \end{aligned}$$

which implies that $\frac{d}{dt} \overline{\mathbf{U}}_j = \mathbf{0}$.

On the other hand, in order to prove $\frac{d}{dt} \mathbf{V}_j = \mathbf{0}$, we need to figure out the classification of equilibrium states. Following [7, 12, 25, 32], we can classify all steady states based on Froude number $Fr := \frac{|u|}{\sqrt{gh}}$. If $Fr > 1$ ($Fr < 1$), the flow is called supercritical (subcritical). If $Fr = 1$, the flow corresponds to the critical case. Since (2.33) is satisfied at every point in space, it also depends on the bottom topography $Z(x)$. We can have such a steady state that it is entirely supercritical or subcritical or a combined one, which is supercritical in one part of the domain and subcritical in another. The latter one is termed transcritical. We then proceed case by case as follows.

We begin with the supercritical flow, of which $Fr = \frac{|u_j|}{\sqrt{gh_j}} > 1$ for all j . Therefore, we will have either $u_j > \sqrt{gh_j} > 0$ or $u_j < -\sqrt{gh_j} < 0$. Without loss of generality, we take into account $u_j > \sqrt{gh_j}$. From (2.10) and (2.12), it is easy to obtain that $J(\mathbf{V}_j)^- = 0$, $\tilde{J}(\mathbf{V}_j)^- = 0$,

$$J(\mathbf{V}_j)^+ = \Upsilon_j \begin{pmatrix} 0 & 0 & 0 \\ 0 & u_j - \sqrt{gh_j} & 0 \\ 0 & 0 & u_j + \sqrt{gh_j} \end{pmatrix} \Upsilon_j^{-1} = \begin{pmatrix} u_j & h_j & 0 \\ g & u_j & g \\ 0 & 0 & 0 \end{pmatrix},$$

and

$$\tilde{J}(\mathbf{V}_j)^+ = \Upsilon_j \begin{pmatrix} 0 & 0 & 0 \\ 0 & 1 & 0 \\ 0 & 0 & 1 \end{pmatrix} \Upsilon_j^{-1} = \begin{pmatrix} 1 & 0 & -\frac{gh_j}{u_j^2 - gh_j} \\ 0 & 1 & \frac{gu_j}{u_j^2 - gh_j} \\ 0 & 0 & 0 \end{pmatrix}.$$

Therefore, according to (2.9), we can get

$$\overleftarrow{\Phi} \mathbf{v}_{j+\frac{1}{2}} = \mathbf{0} \quad (2.35)$$

and

$$\begin{aligned} \overrightarrow{\Phi} \mathbf{v}_{j-\frac{1}{2}} &= \begin{pmatrix} u_j & h_j & 0 \\ g & u_j & g \\ 0 & 0 & 0 \end{pmatrix} \begin{pmatrix} \delta_j^+ h \\ \delta_j^+ u \\ \delta_j^+ Z \end{pmatrix} - \begin{pmatrix} 1 & 0 & -\frac{gh_j}{u_j^2 - gh_j} \\ 0 & 1 & \frac{gu_j}{u_j^2 - gh_j} \\ 0 & 0 & 0 \end{pmatrix} \begin{pmatrix} 0 \\ -\delta_j^+ Q \\ 0 \end{pmatrix} \\ &= \begin{pmatrix} u_j \delta_j^+ h + h_j \delta_j^+ u_j \\ u_j \delta_j^+ u + g(\delta_j^+ h + \delta_j^+ Z) + \delta_j^+ Q \\ 0 \end{pmatrix} \stackrel{(2.22)}{=} \begin{pmatrix} \delta_j^+ q \\ \delta_j^+ E \\ 0 \end{pmatrix}. \end{aligned}$$

Since the data satisfies (2.33), the FD approximations in (2.21) result in

$$\overrightarrow{\Phi} \mathbf{v}_{j-\frac{1}{2}} = \begin{pmatrix} 0 \\ 0 \\ 0 \end{pmatrix},$$

which together with (2.35) implies that $\frac{d}{dt} \mathbf{V}_j = \mathbf{0}$.

We then consider the subcritical case that $Fr = \frac{|u_j|}{\sqrt{gh_j}} < 1$ for all j and it corresponds to $-\sqrt{gh_j} < u_j < \sqrt{gh_j}$. According to (2.10) and (2.12), we will have

$$\Lambda^+ = \begin{pmatrix} 0 & 0 & 0 \\ 0 & 0 & 0 \\ 0 & 0 & u_j + \sqrt{gh_j} \end{pmatrix}, \quad \tilde{\Lambda}^+ = \begin{pmatrix} 0 & 0 & 0 \\ 0 & 0 & 0 \\ 0 & 0 & 1 \end{pmatrix}$$

and thus we get

$$\begin{aligned} J(\mathbf{V}_j)^+ &= \Upsilon_j \Lambda^+ \Upsilon_j^{-1} = \begin{pmatrix} \frac{u_j + \sqrt{gh_j}}{2} & \frac{u_j + \sqrt{gh_j}}{2} \sqrt{\frac{h_j}{g}} & \frac{\sqrt{gh_j}}{2} \\ \frac{u_j + \sqrt{gh_j}}{2} \sqrt{\frac{g}{h_j}} & \frac{u_j + \sqrt{gh_j}}{2} & \frac{g}{2} \\ 0 & 0 & 0 \end{pmatrix}, \\ \tilde{J}(\mathbf{V}_j)^+ &= \Upsilon_j \tilde{\Lambda}^+ \Upsilon_j^{-1} = \begin{pmatrix} \frac{1}{2} & \frac{1}{2} \sqrt{\frac{h_j}{g}} & \frac{\sqrt{gh_j}}{2(u_j + \sqrt{gh_j})} \\ \frac{1}{2} \sqrt{\frac{g}{h_j}} & \frac{1}{2} & \frac{g}{2(u_j + \sqrt{gh_j})} \\ 0 & 0 & 0 \end{pmatrix}. \end{aligned} \quad (2.36)$$

Analogously, we have

$$\Lambda^- = \begin{pmatrix} 0 & 0 & 0 \\ 0 & u_j - \sqrt{gh_j} & 0 \\ 0 & 0 & 0 \end{pmatrix}, \quad \tilde{\Lambda}^- = \begin{pmatrix} 0 & 0 & 0 \\ 0 & 1 & 0 \\ 0 & 0 & 0 \end{pmatrix},$$

and it follows that

$$\begin{aligned}
J(\mathbf{V}_j)^- &= \Upsilon_j \Lambda^- \Upsilon_j^{-1} = \begin{pmatrix} \frac{u_j - \sqrt{gh_j}}{2} & -\frac{u_j - \sqrt{gh_j}}{2} \sqrt{\frac{h_j}{g}} & -\frac{\sqrt{gh_j}}{2} \\ -\frac{u_j - \sqrt{gh_j}}{2} \sqrt{\frac{g}{h_j}} & \frac{u_j - \sqrt{gh_j}}{2} & \frac{g}{2} \\ 0 & 0 & 0 \end{pmatrix}, \\
\tilde{J}(\mathbf{V}_j)^- &= \Upsilon_j \tilde{\Lambda}^- \Upsilon_j^{-1} = \begin{pmatrix} \frac{1}{2} & -\frac{1}{2} \sqrt{\frac{h_j}{g}} & -\frac{\sqrt{gh_j}}{2(u_j - \sqrt{gh_j})} \\ -\frac{1}{2} \sqrt{\frac{g}{h_j}} & \frac{1}{2} & \frac{g}{2(u_j - \sqrt{gh_j})} \\ 0 & 0 & 0 \end{pmatrix}.
\end{aligned} \tag{2.37}$$

Then, by substituting (2.36) and (2.37) into (2.9) and using the relations in (2.22), we obtain

$$\overleftarrow{\Phi}_{j+\frac{1}{2}} \mathbf{V}_{j+\frac{1}{2}} = \begin{pmatrix} \frac{1}{2} \delta_j^- q - \frac{\sqrt{h_j/g}}{2} \delta_j^- E \\ -\frac{\sqrt{g/h_j}}{2} \delta_j^- q + \frac{1}{2} \delta_j^- E \\ 0 \end{pmatrix} \tag{2.38}$$

and

$$\overrightarrow{\Phi}_{j-\frac{1}{2}} \mathbf{V}_{j-\frac{1}{2}} = \begin{pmatrix} \frac{1}{2} \delta_j^+ q + \frac{\sqrt{h_j/g}}{2} \delta_j^+ E \\ \frac{\sqrt{g/h_j}}{2} \delta_j^+ q + \frac{1}{2} \delta_j^+ E \\ 0 \end{pmatrix}. \tag{2.39}$$

Since the data are at the discrete steady state (2.33), from (2.7), we can induce that $\delta_j^\pm q = 0$ and $\delta_j^\pm E = 0$. Therefore, (2.38) and (2.39) reduce to

$$\overleftarrow{\Phi}_{j+\frac{1}{2}} \mathbf{V}_{j+\frac{1}{2}} = \mathbf{0} \quad \text{and} \quad \overrightarrow{\Phi}_{j-\frac{1}{2}} \mathbf{V}_{j-\frac{1}{2}} = \mathbf{0},$$

which is then plugged in (2.8) and end up with $\frac{d}{dt} \mathbf{V}_j = \mathbf{0}$.

Finally, for the transcritical case, since it is a combination of the aforementioned two cases in space, we can omit the WB property verification for this case and complete the proof of the theorem. \blacksquare

Remark 2.5 *As shown in Theorem 2.4, we note that the proposed new WB schemes are capable of exactly preserving all of the still-water equilibria (1.5) and the frictionless moving-water equilibria (1.6). When some moving-water equilibria with nonzero Manning coefficient ($n \neq 0$) are considered, the proposed schemes are only designed to exactly preserve particular discrete versions of the general steady states (1.3) with $u \neq 0$. This is due to the fact that, in this situation, we have applied the third-order Simpson's quadratures to approximate the point values $\{Q_j\}$ in (2.15), which is then used in the evaluation of the discrete steady states to be preserved. Therefore, when the WB property is experimentally verified for the frictional case with nonzero velocity, the initial data should be prepared so that they will satisfy the corresponding discrete steady states. Although this is not yet completely satisfactory, it seems to be a common situation encountered in many existing methods; see, e.g., [7, 11, 29, 31]. We will further explain the data preparation for this case in Example 6.*

2.2 Positivity-Preserving and Nonlinear Stability

In addition to achieve the WB property, it is also great important to preserve the positivity of water depth, as it is not only necessary for physical significance, but also crucial for theoretical analysis and numerical stability. For the proposed schemes, both the cell averages $\{\bar{h}_{j+\frac{1}{2}}\}$ and the point values $\{h_j\}$ should keep positivity. We achieve this goal as follows.

For one thing, in order to ensure that the proposed scheme in (2.5) remains the positivity of the cell averages of water depth, we implement a “draining time step” technique, which was introduced in [6] and then used in [5, 8, 17, 26]. Namely, we replace the numerical fluxes in (2.6) with

$$\mathcal{F}_j = \begin{pmatrix} \frac{\Delta t_j}{\Delta t} q_j \\ \frac{\Delta t_j}{\Delta t} (h_j u_j^2) + \frac{g}{2} h_j^2 \\ 0 \end{pmatrix}, \quad (2.40)$$

where we set the effective time step on the cell interface as

$$\Delta t_j = \min(\Delta t, \Delta t_i^{\text{drain}}), \quad i = j - \frac{\text{sgn}(\mathcal{F}_j^{(1)})}{2}. \quad (2.41)$$

Here, $\Delta t_{j+\frac{1}{2}}^{\text{drain}}$ is the introduced drain time step defined in element $K_{j+\frac{1}{2}}$ with the known average $\bar{h}_{j+\frac{1}{2}}^n$ at the time level $t = t^n$:

$$\Delta t_{j+\frac{1}{2}}^{\text{drain}} := \frac{\Delta x \bar{h}_{j+\frac{1}{2}}^n}{\max(0, \mathcal{F}_{j+1}^{(1)}) + \max(0, -\mathcal{F}_j^{(1)})}.$$

In (2.40) and (2.41), Δt is an adaptive time step and will be determined later.

For another thing, we note that the fluctuation (2.21) and the proposed scheme in §2.1 is not positivity preserving when the non-conservative system (2.3)–(2.4) is solved. In order to ameliorate this flaw so that $h_j \geq 0$ and $h_{j+\frac{1}{2}} \geq 0$, following the idea presented in [1], we design an alternative scheme, which has a Local Lax-Friedrichs’ flavor and a positivity preserving property for the water depth at the cell interface. To this end, we first rewrite the studied nonconservative system (1.7) as

$$\begin{cases} h_t + q_x = 0, \\ u_t + E_x = 0. \end{cases} \quad (2.42)$$

Then, the point values $\{h_j\}$ and $\{u_j\}$ are evolved in time using the following semi-discretization:

$$\frac{d}{dt} \mathbb{V}_j = -(\overleftarrow{\Phi}_{j+\frac{1}{2}}^{\mathbb{V}} + \overrightarrow{\Phi}_{j-\frac{1}{2}}^{\mathbb{V}}), \quad \mathbb{V}_j = (h_j, u_j)^\top, \quad (2.43)$$

where

$$\overleftarrow{\Phi}_{j+\frac{1}{2}}^{\mathbb{V}} = \frac{1}{\Delta x} \begin{pmatrix} q_{j+\frac{1}{2}} - q_j - \alpha \Gamma_{j+\frac{1}{2}} (h_{j+\frac{1}{2}} - h_j) \\ E_{j+\frac{1}{2}} - E_j - \alpha \Gamma_{j+\frac{1}{2}} (u_{j+\frac{1}{2}} - u_j) \end{pmatrix} \quad (2.44)$$

and

$$\overrightarrow{\Phi}_{j+\frac{1}{2}}^{\mathbb{V}} = \frac{1}{\Delta x} \begin{pmatrix} q_{j+1} - q_{j+\frac{1}{2}} - \alpha \Gamma_{j+\frac{1}{2}} (h_{j+\frac{1}{2}} - h_{j+1}) \\ E_{j+1} - E_{j+\frac{1}{2}} - \alpha \Gamma_{j+\frac{1}{2}} (u_{j+\frac{1}{2}} - u_{j+1}) \end{pmatrix}. \quad (2.45)$$

For the sake of simplicity and as well as ensuring $h_{j+\frac{1}{2}} \geq 0$, we take $\mathbb{V}_{j+\frac{1}{2}} = \Psi^{-1}(\overline{\mathbf{U}}_{j+\frac{1}{2}})$ here. Namely, we take $h_{j+\frac{1}{2}} = \overline{h}_{j+\frac{1}{2}}$ and $u_{j+\frac{1}{2}} = \overline{q}_{j+\frac{1}{2}}/\overline{h}_{j+\frac{1}{2}}$. For the purpose of consistency, we use these new values and the formulae given in (2.15) and (2.16) to recompute $E_{j+\frac{1}{2}}$. In (2.44) and (2.45), α is an upper-bound of the spectral radius of $J(\mathbb{V}_j)$, $J(\mathbb{V}_{j+\frac{1}{2}})$, and $J(\mathbb{V}_{j+1})$. $\Gamma_{j+\frac{1}{2}} = \mathcal{H}(\eta_{j+\frac{1}{2}}) \in [0, 1]$ is a parameter used to control the numerical diffusion and $\mathcal{H}(\eta)$ is a smooth cut-off function given by

$$\mathcal{H}(\eta) := \frac{(C\eta)^m}{1 + (C\eta)^m},$$

which is relatively small when the computed solution is locally (almost) at a steady state, while rapidly approaches 1 when the solution is away from the steady state. In all of the numerical experiments reported in section 3, we have used the constants $C = 6$, $m = 20$, and taken

$$\eta_{j+\frac{1}{2}} := \frac{E_{j+1} - E_j}{\Delta x} \cdot \frac{\sum_j |K_{j+\frac{1}{2}}|}{\max(E_{j+1}, E_j)}.$$

For more descriptions of this numerical diffusion switch function, we refer to [7, 13, 26].

Finally, as pointed out in [1], the proposed scheme in section 2.1 is at most linearly stable and not positivity-preserving, with a CFL condition based on the fine grid. In order to ensure the positivity of the point values of water depth, we apply the MOOD paradigm which was used in [1, 2, 19, 36] to switch the numerical schemes to the parachute ones. The idea is to work with several schemes ordered from the most accurate/less stable one to the low order/more reliable one, which is a parachute scheme and able to provide solutions fulfilling some criteria. These detection criteria are set up according to the computer, physical, and numerical admissibility. For example, no NaN (Not-a-Number) and positive water depth are considered here.

In this work, we use the simplified version of the MOOD algorithm, that is, only the third order new scheme defined in section 2.1 and the first order local Lax Friedrichs scheme defined above are taken into account. We expect to use as often as possible the third order scheme, and to use the first order one to correct potential problems. Therefore, we first perform a step of the higher accurate scheme, and then check the criteria on each cell to detect the areas where the criteria are not met. Next, on these troubled cells, we switch to the parachute scheme in a cascade style. We proceed iteratively until either the criteria are met or the most reliable/less accurate parachute scheme is used. We illustrate this procedure in Figure 2.1.

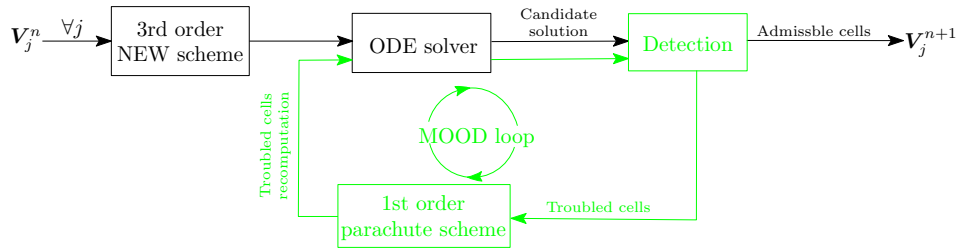


Figure 2.1: Sketch of the proposed WB NEW scheme stabilized by a MOOD loop.

We now establish the detection criteria to complete the description of MOOD paradigm:

1. We check if all of the primitive variables are numbers (i.e., not NaN and not Inf). If this holds, the criterion is set to `.TRUE.` and we look for the next criterion, else it is set to `.FALSE.` and we jump to the next element;

2. We check if the water depth is positive. If not, we set the criterion to `.FALSE.` and jump to the next element. Otherwise, we set the criterion to `.TRUE.` and check next criterion.

Remark 2.6 *When the low-order parachute scheme is triggered, for consistency, we will replace the computations in (2.15) and (2.26) with the corresponding low-order approximations:*

$$Q_{j+1} = Q_j + \int_{x_j}^{x_{j+1}} \frac{gn^2}{h^{\frac{4}{3}}} |u|u \, dx \approx Q_j + \frac{gn^2 \Delta x |u_{j+\frac{1}{2}}| u_{j+\frac{1}{2}}}{(h_{j+\frac{1}{2}})^{4/3}}$$

and

$$\overline{S}_{j+\frac{1}{2}}^{(2)} \approx \frac{1}{\Delta x} \left[h_{j+1} u_{j+1}^2 - h_j u_j^2 + \frac{g}{2} (h_{j+1}^2 - h_j^2) \right] - \frac{u_j + u_{j+1}}{2} (q_x)_{j+\frac{1}{2}} - \frac{h_j + h_{j+1}}{2} (E_x)_{j+\frac{1}{2}},$$

respectively.

3 Numerical Examples

In this section, we demonstrate the performance of the proposed new WB schemes on several numerical examples. In some of the following examples, we compare the numerical results obtained by the developed new WB schemes with those computed by the WB central-upwind scheme from [7]. For the sake of simplicity, we refer to the former as “NEW scheme” and the latter as “OLD scheme”. In all numerical experiments, unless specified otherwise, we assume that the acceleration due to gravity $g = 9.812$ and use zero-order extrapolation boundary conditions. The figures presented below plot the cell average values of the variables of interest.

In the numerical implementation, we integrate the ODE systems (2.5) and either (2.8) or (2.43) using the three-stage third-order strong stability preserving (SSP) Runge-Kutta method (see, e.g., [22, 23]) with an adaptive time step computed at every time level using the CFL number 0.4, namely, by taking

$$\Delta t = 0.4 \frac{\Delta x}{a_{\max}},$$

where a_{\max} is an upper-bound of the spectral radius of $J(\mathbf{V}_j)$, $J(\mathbf{V}_{j+\frac{1}{2}})$, and $J(\mathbf{V}_{j+1})$.

3.1 Frictionless Saint-Venant System ($n = 0$)

We begin with five examples for the frictionless Saint-Venant system (1.1) with $n = 0$. In this case, both the still-water (1.5) and moving-water (1.6) equilibria can be exactly preserved by the WB schemes.

Example 1—Accuracy Test

The goal of the first example is to numerically check the experimental rate of convergence. To this end, we consider the following initial data and bottom topography taken from [4]:

$$h(x, 0) = 0.3 \left[1 + e^{-\frac{(x-0.5)^2}{0.05^2}} \right] - 0.2 \cos(6\pi x), \quad q(x, 0) = 0, \quad Z(x) = 0.2(1 + \cos(6\pi x)),$$

which is prescribed in a computational domain $[0, 1]$ and subject to the periodic boundary conditions.

We first use a numerical solution at the final time $t = 0.03$ computed by the NEW scheme on a substantial fine mesh with 16384 uniform cells as a reference solution, since the exact solution is not explicitly known for this initial-boundary value problem. We then run the same simulations but with different number of grids. Namely, we take 64, 128, 256, 512, 1024, 2048, and 4096 uniform grids to generate the numerical solutions. Finally, we measure the discrete L^1 -errors for both h and q at the cell interfaces. The obtained results are reported in Table 3.1, which shows the expected experimental third order of accuracy.

Table 3.1: Example 1: L^1 -errors and experimental convergence rates.

Δx	L^1 -error in h	Rate	L^1 -error in q	Rate
1/64	2.20×10^{-4}	–	4.03×10^{-4}	–
1/128	5.90×10^{-5}	1.90	1.15×10^{-4}	1.81
1/256	8.79×10^{-6}	2.75	1.80×10^{-5}	2.67
1/512	1.26×10^{-6}	2.80	2.64×10^{-6}	2.77
1/1024	1.75×10^{-7}	2.85	3.82×10^{-7}	2.79
1/2048	2.59×10^{-8}	2.76	7.01×10^{-8}	2.44
1/4096	4.22×10^{-9}	2.62	1.28×10^{-8}	2.46

Example 2—Still-Water Equilibrium and Its Small Perturbation

In the second example, we validate that the NEW schemes are capable of exactly preserving the still-water steady state. To this end, we take the bottom topography

$$Z(x) = \begin{cases} 2(\cos(10\pi(x + 0.3)) + 1), & x \in [-0.4, -0.2], \\ 0.5(\cos(10\pi(x - 0.3)) + 1), & x \in [0.2, 0.4], \\ 0, & \text{otherwise,} \end{cases}$$

and consider the following initial data

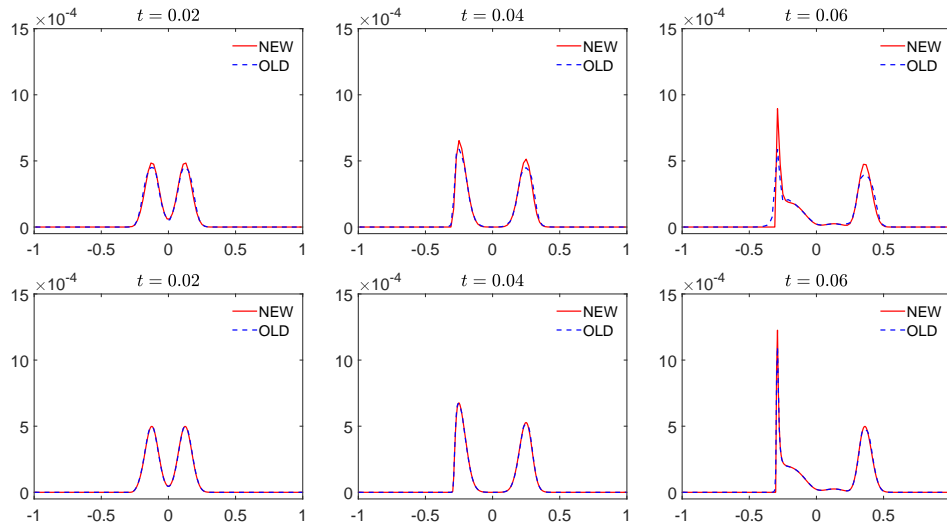
$$h(x, 0) := h_{\text{eq}}(x) = 4.000001 - Z(x), \quad q(x, 0) := q_{\text{eq}}(x) = 0,$$

which satisfies (1.5) in the computational domain $[-1, 1]$. We run the simulations until a long final time $t = 30$ using both the NEW and OLD schemes with 100 uniform cells. Then we calculate the L^1 - and L^∞ -errors in h and q and report the obtained errors in Table 3.2. As one can clearly see, both of the two studied schemes can preserve the still-water steady state at the level of round-off error.

We now add a small Gaussian-shape perturbation to the stationary water depth and test the ability of the proposed schemes to accurately capture this small perturbation. In order to compare with the OLD scheme that a WB method is developed based on finite volume framework, we only

Table 3.2: Example 2: L^1 - and L^∞ -errors in h and q computed by the NEW and OLD schemes.

	L^1 -error in h	L^∞ -error in h	L^1 -error in q	L^∞ -error in q
NEW scheme	6.92e-14	3.82e-14	2.03e-13	2.19e-13
OLD scheme	2.33e-15	2.22e-15	3.45e-14	3.16e-14

Figure 3.1: Example 2 (small perturbation): Time snapshots of the difference $h - h_{\text{eq}}$ computed by the NEW and OLD schemes using a coarse mesh with 100 cells (top row) and a finer mesh with 300 cells (bottom row).

“pollute” the cell average of water depth. That is, we add a small perturbation, which takes the form of $10^{-3}e^{-200x^2}$, to the initial cell average of water depth and compute the numerical solutions at three different times $t = 0.02, 0.04,$ and 0.06 using either 100 or 300 uniform cells by both the NEW and OLD schemes. The differences between the computed and background cell averages of water depth are plotted in Figure 3.1. As one can observe, the initial perturbation splits into two humps, which are then propagating into opposite directions, respectively. When the coarse mesh is used, the NEW scheme generates much more accurate results. In particular, at the final time $t = 0.06$, the difference at $x \approx 0.3$ computed by the NEW scheme is much sharper than its counterpart. When the mesh is refined, both of the two studied schemes converge to (almost) the same solution. In addition, we can also conclude that the proposed NEW scheme is positive-preserving, as it can accurately handle cases with smallest water depth $h \approx 10^{-6}$.

Example 3—Moving-Water Equilibria and Their Small Perturbations

In the third example, we verify the WB property of the NEW scheme in the sense that it is capable of exactly preserving moving-water equilibria (1.6). To this end, we consider a continuous bottom topography,

$$Z(x) = \begin{cases} 0.2 - 0.05(x - 10)^2 & \text{if } 8 \leq x \leq 12, \\ 0 & \text{otherwise,} \end{cases} \quad (3.1)$$

prescribed in the computational domain $[0, 25]$ and the following three sets of initial data that correspond to three different flow regimes (supercritical, subcritical, and transcritical without shock):

$$\begin{aligned}
 \text{Case (a): } & q_{\text{eq}}(x, 0) \equiv 24, \quad E_{\text{eq}}(x, 0) \equiv \frac{24^2}{2 \times 2^2} + 9.812 \times 2; \\
 \text{Case (b): } & q_{\text{eq}}(x, 0) \equiv 4.42, \quad E_{\text{eq}}(x, 0) \equiv \frac{4.42^2}{2 \times 2^2} + 9.812 \times 2; \\
 \text{Case (c): } & q_{\text{eq}}(x, 0) \equiv 1.53, \quad E_{\text{eq}}(x, 0) \equiv \frac{3}{2}(9.812 \times 1.53)^{\frac{2}{3}} + 9.812 \times 0.2.
 \end{aligned} \tag{3.2}$$

The relevant steady-state water depths $h_{\text{eq}}(x, 0)$ are computed in the same manner as introduced in [12, Remark 4.1] and given by

$$\begin{aligned}
 \text{Case (a): } & h_{\text{eq}}(x, 0) = -\frac{a_0}{3} \left[2 \cos \left(\frac{\theta + 4\pi}{3} \right) + 1 \right]; \\
 \text{Case (b): } & h_{\text{eq}}(x, 0) = -\frac{a_0}{3} \left[2 \cos \frac{\theta}{3} + 1 \right]; \\
 \text{Case (c): } & h_{\text{eq}}(x, 0) = \begin{cases} -\frac{a_0}{3} \left[2 \cos \left(\frac{\theta + 4\pi}{3} \right) + 1 \right], & x > 10, \\ -\frac{a_0}{3} \left[2 \cos \frac{\theta}{3} + 1 \right], & x < 10, \\ -\frac{2a_0}{3}, & x = 10, \end{cases}
 \end{aligned} \tag{3.3}$$

where $a_0 = \frac{gZ(x) - E_{\text{eq}}(x, 0)}{g}$, $a_2 = \frac{(q_{\text{eq}}(x, 0))^2}{2g}$, and $\theta = \arccos(1 + \frac{27a_2}{2a_0^3})$.

We first use the NEW scheme with 100 uniform cells to compute the numerical solutions until a final time $t = 20$ for all three cases mentioned above. The discrete L^1 - and L^∞ -errors in h and q are computed and reported in Table 3.3. It is clear that the NEW scheme can exactly preserve all three moving-water equilibria within machine accuracy.

Table 3.3: Example 3: L^1 - and L^∞ -errors in h and q computed by the NEW scheme.

	L^1 -error in h	L^∞ -error in h	L^1 -error in q	L^∞ -error in q
Case (a)	3.65e-13	3.69e-14	3.53e-12	3.69e-13
Case (b)	3.80e-14	7.99e-15	5.73e-13	5.33e-14
Case (c)	2.15e-14	2.78e-15	6.70e-14	9.10e-15

We then add a small perturbation, which takes the form of $10^{-3}e^{-80(x-6)^2}$, to the steady-state cell average of water depth $h_{\text{eq}}(x, 0)$ in (3.3). We compute the numerical solutions using the NEW and OLD schemes until $t = 1$ in the supercritical case and until $t = 1.5$ in the subcritical and transcritical cases. The difference between the obtained and the background moving steady-state cell averages of water depth computed with 100 and 1000 uniform cells are plotted in Figure 3.2. As one can observe, the propagating perturbations are well captured by both studied schemes over both coarse and fine meshes. Comparing the results obtained by different schemes, we can see that the NEW scheme produces much higher resolution solutions.

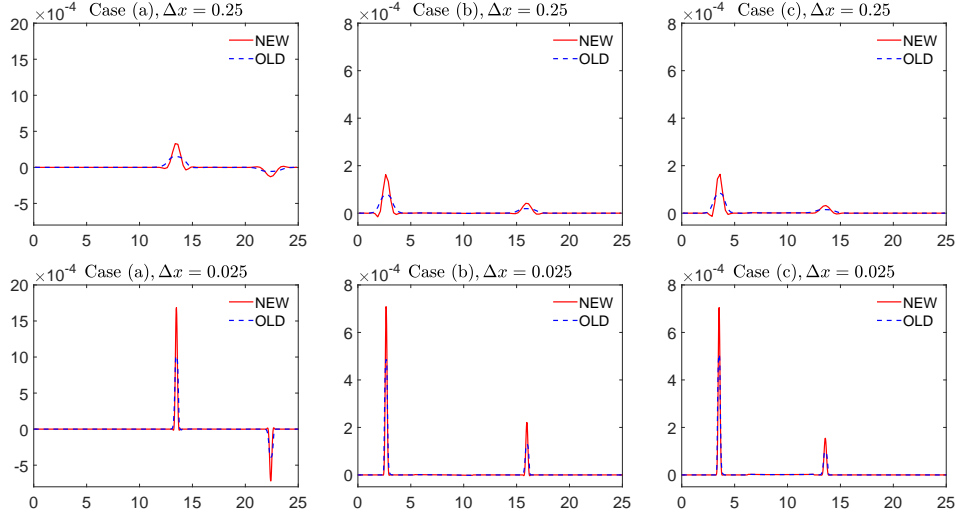


Figure 3.2: Example 3: The difference between the obtained and the steady-state cell averages of water depth computed by both the NEW and OLD schemes using uniform cells with mesh size $\Delta x = 0.25$ (top row) and $\Delta x = 0.025$ (bottom row) for Cases (a, left column), (b, middle column) and (c, right column).

Example 4—Convergence to Moving-Water Equilibria

In the fourth example, we study the convergence in time of the numerical solution computed by the proposed NEW scheme towards steady flow over a continuous hump given by (3.1). Depending on the initial and boundary conditions, the obtained convergent flow may be supercritical, subcritical, or transcritical without or with a steady shock. The four sets of initial and boundary conditions in terms of water depth and velocity are summarized as follows:

$$\begin{aligned}
 \text{Case (a):} & \quad \begin{cases} h(x, 0) = 2 - Z(x), & u(x, 0) = 0, \\ h(0, t) = 2, & u(0, t) = 12; \end{cases} \\
 \text{Case (b):} & \quad \begin{cases} h(x, 0) = 2 - Z(x), & u(x, 0) = 0, \\ h(0, t) = 2, & u(0, t) = 2.21, \quad h(25, t) = 2; \end{cases} \\
 \text{Case (c):} & \quad \begin{cases} h(x, 0) = 0.66 - Z(x), & u(x, 0) = 0, \\ h(0, t) = 1.01439, & u(0, t) = 1.53/h(0, t), \quad h(25, t) = 0.66; \end{cases} \\
 \text{Case (d):} & \quad \begin{cases} h(x, 0) = 0.33 - Z(x), & u(x, 0) = 0, \\ h(0, t) = 0.41372, & u(0, t) = 0.18/h(0, t), \quad h(25, t) = 0.33. \end{cases}
 \end{aligned}$$

Remark 3.1 *In Case (c), the downstream boundary condition ($h(25, t) = 0.66$) is imposed only when the flow is subcritical.*

The numerical solutions ($h + Z$, q , and E) at a final time $t = 500$ on the computational domain $[0, 25]$ computed by the NEW scheme with 200 uniform cells are depicted in Figure 3.3. As one can see, the numerical solutions of the first three cases have almost converged to the desired discrete steady states. However, for Case (d), like most of the existing schemes, the proposed scheme also

fails to accurately resolve the equilibrium as the errors at the shock are $\mathcal{O}(1)$. It is easy to find that the numerical solutions obtained here are comparable with those reported in [7, 11, 12, 29].

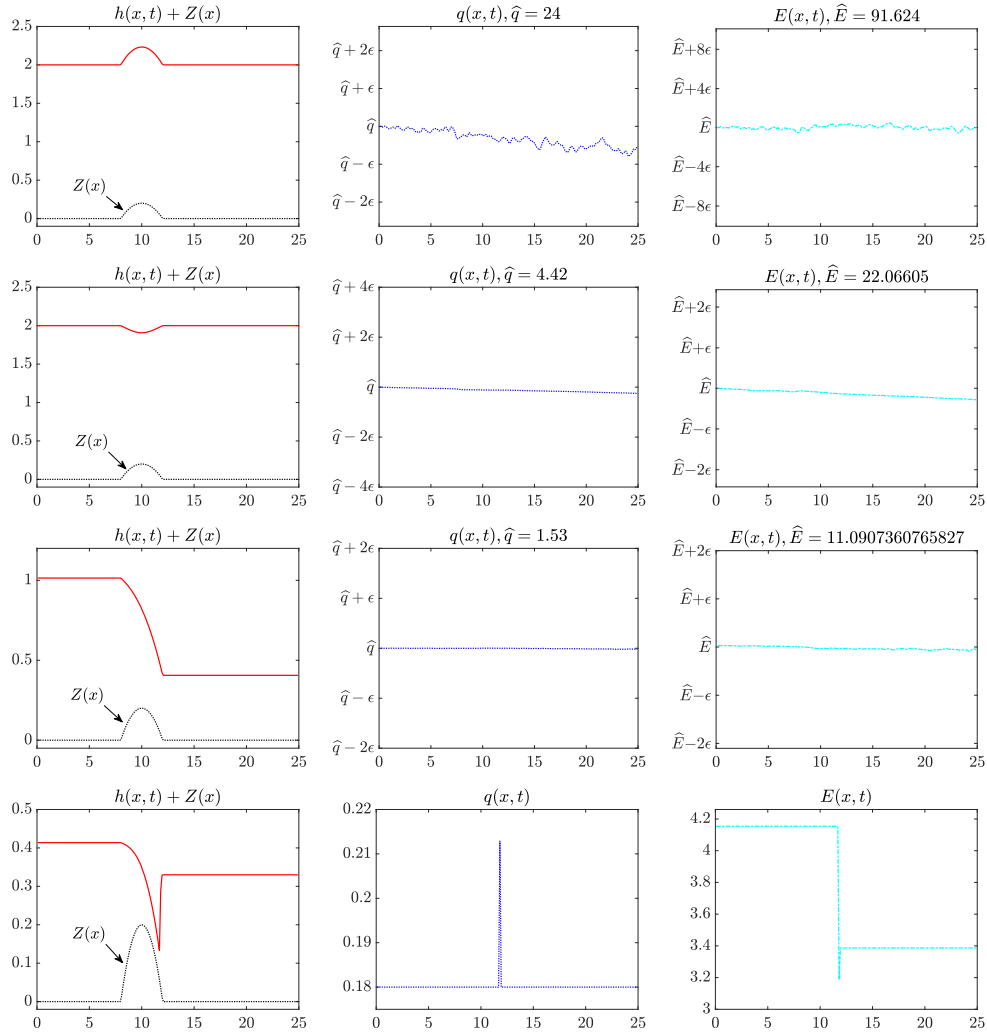


Figure 3.3: Example 4: Convergent solutions of $h + Z$ together with Z (left column), q (middle column) and E (right column) for Cases (a, first row), (b, second row), (c, third row), and (d, fourth row). The small deviation parameter $\epsilon = 10^{-12}$.

Example 5—Two Rarefaction Waves Problem

In the fifth example taken from [35], we study a problem associated with two rarefaction waves moving toward opposite directions. The initial data and bottom topography are

$$(h(x, 0), u(x, 0), Z(x)) = \begin{cases} (8, -2, 0), & x < 0, \\ (5, 7.1704, 1), & x \geq 0. \end{cases}$$

The exact solution of this problem is given by a left-propagating 1-Rarefaction, a bottom step discontinuity, and a right-propagating 2-Rarefaction. We use both the NEW and OLD schemes to compute the numerical solutions at the final time $t = 8$ in the computational domain $[-150, 150]$

covered with 300 uniform cells. Results are shown in Figure 3.4. As one can see, the obtained water surface $h + Z$ profiles provide expected results with a left-directed rarefaction wave, a stationary shock, and a right-directed rarefaction wave. The numerical solutions computed by the two studied schemes are in satisfactory agreement.

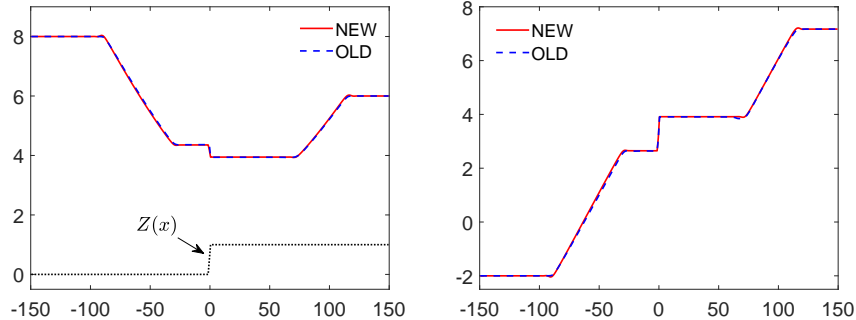


Figure 3.4: Example 5: Water surface $h + Z$ together with Z (left) and velocity u (right) computed by the NEW and OLD schemes.

3.2 Saint-Venant System with Friction ($n \neq 0$)

We present two additional numerical examples for the Saint-Venant system (1.1) with a nonzero Manning coefficient. That is, in the two numerical examples considered below, we take $n = 0.05$.

Example 6—Convergence to Moving-Water Equilibria and Their Small Perturbations

In the sixth example, which is a modification of Example 4, we now consider a nonzero Manning friction term and study the convergence in time of the numerical solution towards discrete steady states over a continuous hump given by (3.1). Three cases corresponding to the supercritical [Case (a)], subcritical [Case (b)], and transcritical flow with a steady shock [Case (d)] are taken into account. We take “lake-at-rest” initial conditions and the Dirichlet boundary conditions:

$$\begin{aligned} \text{Case (a):} & \begin{cases} h(x, 0) = 2 - Z(x), & u(x, 0) = 0, \\ h(0, t) = 2, & u(0, t) = 12; \end{cases} \\ \text{Case (b):} & \begin{cases} h(x, 0) = 2 - Z(x), & u(x, 0) = 0, \\ h(0, t) = 2.14618, & u(0, t) = 4.42/h(0, t), \quad h(25, t) = 2; \end{cases} \\ \text{Case (d):} & \begin{cases} h(x, 0) = 0.33 - Z(x), & u(x, 0) = 0, \\ h(0, t) = 0.44835, & u(0, t) = 0.18/h(0, t), \quad h(25, t) = 0.32. \end{cases} \end{aligned}$$

As in Example 4, we compute the numerical solutions using the proposed NEW scheme at time $t = 500$ in the computational domain $[0, 25]$ covered with 200 uniform cells. We plot the obtained numerical solutions ($h + Z$, q , and E) in Figure 3.5. As one can see, the obtained numerical results are comparable with those reported in [11, 29]. We can therefore conclude that the proposed NEW

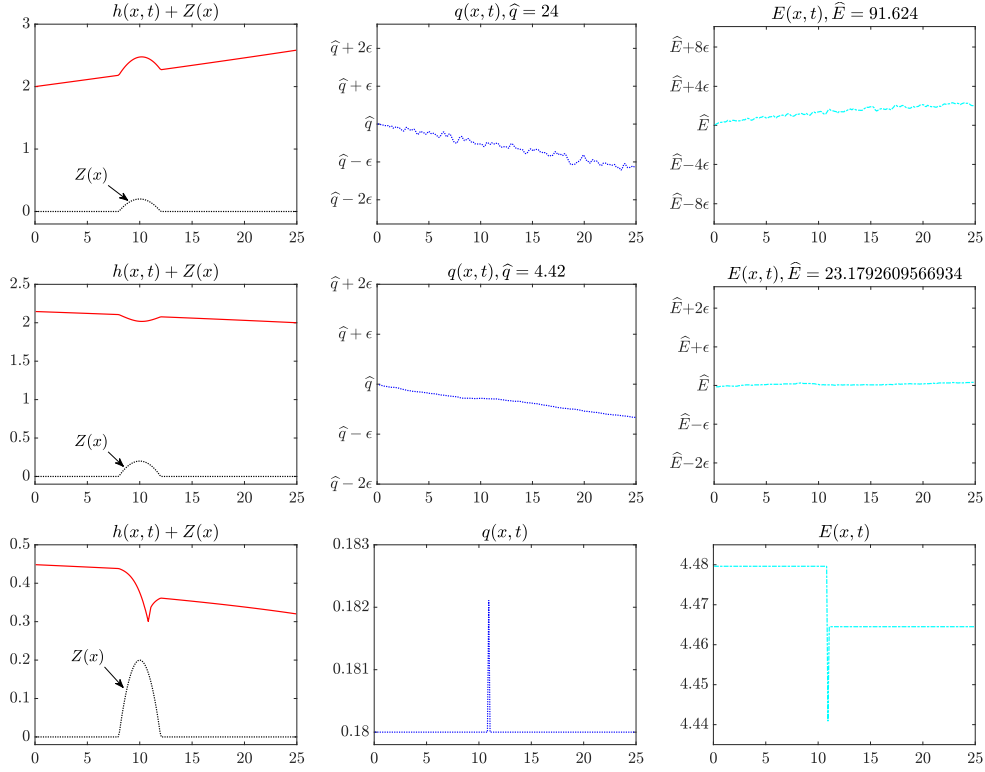


Figure 3.5: Example 6: Convergent solutions of $h + Z$ together with Z (left column), q (middle column) and E (right column) for Cases (a, first row), (b, middle row), and (d, bottom row) with $n = 0.05$ and the deviation number $\epsilon = 10^{-12}$.

scheme is also able to capture the steady states of different flow regimes in the presence of nonzero friction terms. This also confirms the explanation given in Remark 2.5.

We then test the ability of the proposed NEW scheme to capture small perturbations of the obtained discrete steady states of Cases (a) and (b). Similar to Example 3, we add a small perturbation $10^{-3}e^{-80(x-6)^2}$ to the discrete steady-state cell average of water depth obtained from the following two sets of the discrete moving-water equilibria:

$$\begin{aligned} \text{Case (a): } & q(x, 0) \equiv 24, & E(x, 0) & \equiv 91.624; \\ \text{Case (b): } & q(x, 0) \equiv 4.42, & E(x, 0) & \equiv 23.1792609566934. \end{aligned} \quad (3.4)$$

We note that the initial data in (3.4) is given in terms of the equilibrium variable $\mathbf{E} = (q, E)^\top$ rather than in h and u . However, in order to start the computation at time $t = 0$, one has to obtain the average values of $\bar{h}_{j+\frac{1}{2}}$ and the point values of h_j . Unlike Example 3, here we use the Newton's method to numerically solve the following nonlinear equations:

$$E_j = \frac{q_j^2}{2h_j^2} + g(h_j + Z_j) + Q_j, \quad \bar{E}_{j+\frac{1}{2}} = \frac{\bar{q}_{j+\frac{1}{2}}}{2\bar{h}_{j+\frac{1}{2}}^2} + g(\bar{h}_{j+\frac{1}{2}} + \bar{Z}_{j+\frac{1}{2}}) + Q_{j+\frac{1}{2}}, \quad \forall j,$$

where $Q_{j+\frac{1}{2}} = \frac{1}{2}(Q_j + Q_{j+1})$ and $\{Q_j\}_{j>1}$ are computed from the recursive formula (2.15). After obtaining the values of water depth, it is easy to compute the initial values of velocity. Namely, we take $\bar{u}_{j+\frac{1}{2}} = \bar{q}_{j+\frac{1}{2}}/\bar{h}_{j+\frac{1}{2}}$ and $u_j = q_j/h_j$.

Equipped with the initial values in terms of water depth and velocity, we now compute the numerical solutions using the NEW scheme until $t = 1$ and $t = 1.5$ for Cases (a) and (b), respectively. The difference between the computed and the background discrete moving steady-state cell averages of water depth are plotted in Figure 3.6, where one can see that the proposed NEW scheme is able to accurately capture the small perturbation in a robust manner.

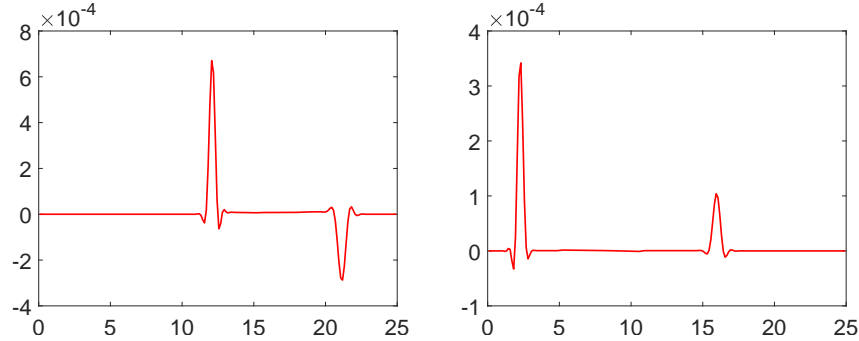


Figure 3.6: Example 6: The difference between the computed and the background discrete steady-state cell averages of water depth computed using 200 uniform cells for Cases (a, left) and (b, right).

Example 7—Riemann Problem

The final example taken from [11, 29] is used to verify the positivity-preserving property of the NEW scheme. To this end, we consider the following initial value problem in $[0, 25]$ with the Riemann initial data:

$$h(x, 0) = \begin{cases} 2 & \text{if } x < 5, \\ 0 & \text{otherwise,} \end{cases} \quad u(x, 0) = \begin{cases} 12 & \text{if } x < 5, \\ 0 & \text{otherwise,} \end{cases}$$

subject to the Dirichlet boundary condition:

$$h(0, t) = 2, \quad u(0, t) = 12.$$

The bottom topography is given by (3.1). We compute the solutions using 100 uniform cells at five different times: $t = 0.2, 0.5, 1, 2,$ and 6 . The numerical solutions ($h + Z$, q , and E) of these time snapshots are plotted in Figure 3.7. As one can clearly observe that the water flow runs through the bottom hump and by $t = 6$ it reaches the same discrete steady state as in Example 6, case (a) as expected. The obtained results are stable and thus show that the proposed NEW scheme possesses the positivity-preserving property.

4 Conclusion

In this paper, we have developed and tested new positivity-preserving well-balanced schemes for the one-dimensional (1-D) Saint-Venant system of shallow water equations with the Manning friction term. The main challenge in developing an accurate and robust well-balanced scheme for the 1-D shallow water equations is related to the fact that a special transformation between the conservative variables and the equilibrium variables is crucial to recover the moving water

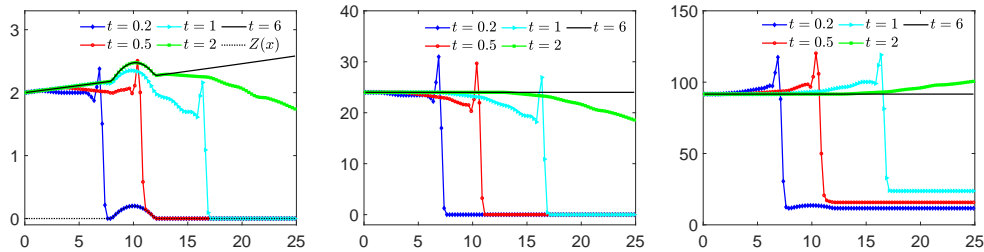


Figure 3.7: Example 7: Computed solutions of $h + Z$ together with Z (left), q (middle) and E (right).

equilibrium; see, e.g., [7, 11, 12, 17, 18, 25, 37]. In the process of transformation, one has to solve some (nonlinear) systems of equations and this can be cumbersome. In order to ameliorate this, we work on both the conservative and non-conservative forms of the studied hyperbolic system. More precisely, we use the former form to evolve the cell averages while we use the latter one to evolve the point values. The novelty of our method is that it only requires solving some linear systems of equations to achieve the transformation from the equilibrium variables to the primitive variables and ensure the well-balanced property. We also propose a way to guarantee the positivity property of cell averages and point values of water depth.

This study is only concerned with the one-dimensional shallow water equations but provides a new framework that is easy to transform from equilibrium variables to primitive variables for designing WB methods. In future work, we plan to extend the method to several space dimensions and other hyperbolic models including the thermal rotating shallow water equations, shallow water flows in channels, and the shallow water flows governing the solute transport process.

Acknowledgment

The work of R. Abgrall and Y. Liu was supported in part by SNF grants 200020_204917 and FZEB-0-166980.

References

- [1] R. ABGRALL, *A combination of Residual Distribution and the Active Flux formulations or a new class of schemes that can combine several writings of the same hyperbolic problem: application to the 1D Euler equation*, Commun. Appl. Math. Comput., 5 (2023), pp. 370–402.
- [2] R. ABGRALL AND D. TORLO, *Some preliminary results on a high order asymptotic preserving computationally explicit kinetic scheme*, Commun. Math. Sci., 20 (2022), pp. 297–326.
- [3] E. AUDUSSE, F. BOUCHUT, M.-O. BRISTEAU, R. KLEIN, AND B. PERTHAME, *A fast and stable well-balanced scheme with hydrostatic reconstruction for shallow water flows*, SIAM J. Sci. Comput., 25 (2004), pp. 2050–2065.
- [4] W. BARSUKOW AND J. P. BERBERICH, *A well-balanced Active Flux method for the shallow water equations with wetting and drying*. <https://doi.org/10.48550/arXiv.2212.02426>.
- [5] A. BOLLERMANN, G. CHEN, A. KURGANOV, AND S. NOELLE, *A well-balanced reconstruction of wet/dry fronts for the shallow water equations*, J. Sci. Comput., 56 (2013), pp. 267–290.

- [6] A. BOLLERMANN, S. NOELLE, AND M. LUKÁČOVÁ-MEDVIĐOVÁ, *Finite volume evolution Galerkin methods for the shallow water equations with dry beds*, Commun. Comput. Phys., 10 (2011), pp. 371–404.
- [7] Y. CAO, A. KURGANOV, Y. LIU, AND R. XIN, *Flux globalization based well-balanced path-conservative central-upwind schemes for shallow water models*, J. Sci. Comput, 92 (2022). Paper No. 69, 31 pp.
- [8] Y. CAO, A. KURGANOV, Y. LIU, AND V. ZEITLIN, *Flux globalization based well-balanced path-conservative central-upwind scheme for two-layer thermal rotating shallow water equations*, J. Comput. Phys., (2023), p. 111790. 29 pp.
- [9] M. J. CASTRO, A. PARDO MILANÉS, AND C. PARÉS, *Well-balanced numerical schemes based on a generalized hydrostatic reconstruction technique*, Math. Models Methods Appl. Sci., 17 (2007), pp. 2055–2113.
- [10] M. J. CASTRO DÍAZ, J. A. LÓPEZ-GARCÍA, AND C. PARÉS, *High order exactly well-balanced numerical methods for shallow water systems*, J. Comput. Phys., 246 (2013), pp. 242–264.
- [11] Y. CHENG, A. CHERTOCK, M. HERTY, A. KURGANOV, AND T. WU, *A new approach for designing moving-water equilibria preserving schemes for the shallow water equations*, J. Sci. Comput., 80 (2019), pp. 538–554.
- [12] Y. CHENG AND A. KURGANOV, *Moving-water equilibria preserving central-upwind schemes for the shallow water equations*, Commun. Math. Sci., 14 (2016), pp. 1643–1663.
- [13] A. CHERTOCK, S. CUI, A. KURGANOV, Ş. N. ÖZCAN, AND E. TADMOR, *Well-balanced schemes for the Euler equations with gravitation: Conservative formulation using global fluxes*, J. Comput. Phys., 358 (2018), pp. 36–52.
- [14] A. CHERTOCK, S. CUI, A. KURGANOV, AND T. WU, *Well-balanced positivity preserving central-upwind scheme for the shallow water system with friction terms*, Int. J. Numer. Methods Fluids, 78 (2015), pp. 355–383.
- [15] A. CHERTOCK, M. DUDZINSKI, A. KURGANOV, AND M. LUKÁČOVÁ-MEDVIĐOVÁ, *Well-balanced schemes for the shallow water equations with Coriolis forces*, Numer. Math., 138 (2018), pp. 939–973.
- [16] A. CHERTOCK, M. HERTY, AND Ş. N. ÖZCAN, *Well-balanced central-upwind schemes for 2×2 systems of balance laws*, in Theory, Numerics and Applications of Hyperbolic Problems I, vol. 236 of Springer Proceedings in Mathematics & Statistics, Springer, 2018, pp. 345–361.
- [17] A. CHERTOCK, A. KURGANOV, X. LIU, Y. LIU, AND T. WU, *Well-balancing via flux globalization: Applications to shallow water equations with wet/dry fronts*, J. Sci. Comput., 90 (2022). Paper No. 9, 21 pp.
- [18] M. CIALLELLA, D. TORLO, AND M. RICCHIUTO, *Arbitrary high order WENO finite volume scheme with flux globalization for moving equilibria preservation*, (2022). arXiv preprint arXiv:2205.13315.

- [19] S. CLAIN, S. DIOT, AND R. LOUBÈRE, *A high-order finite volume method for systems of conservation laws—multi-dimensional optimal order detection (MOOD)*, J. Comput. Phys., 230 (2011), pp. 4028–4050.
- [20] U. S. FJORDHOLM, S. MISHRA, AND E. TADMOR, *Well-balanced and energy stable schemes for the shallow water equations with discontinuous topography*, J. Comput. Phys., 230 (2011), pp. 5587–5609.
- [21] J. GALLARDO, C. PARÉS, AND M. CASTRO, *On a well-balanced high-order finite volume scheme for shallow water equations with topography and dry areas*, J. Comput. Phys., 227 (2007), pp. 574–601.
- [22] S. GOTTLIEB, D. KETCHESON, AND C.-W. SHU, *Strong stability preserving Runge-Kutta and multistep time discretizations*, World Scientific Publishing Co. Pte. Ltd., Hackensack, NJ, 2011.
- [23] S. GOTTLIEB, C.-W. SHU, AND E. TADMOR, *Strong stability-preserving high-order time discretization methods*, SIAM Rev., 43 (2001), pp. 89–112.
- [24] S. JIN AND X. WEN, *Two interface-type numerical methods for computing hyperbolic systems with geometrical source terms having concentrations*, SIAM J. Sci. Comput., 26 (2005), pp. 2079–2101. electronic.
- [25] C. KLINGENBERG, A. KURGANOV, Y. LIU, AND M. ZENK, *Moving-water equilibria preserving HLL-type schemes for the shallow water equations*, Commun. Math. Res., 36 (2020), pp. 247–271.
- [26] A. KURGANOV, Y. LIU, AND V. ZEITLIN, *A well-balanced central-upwind scheme for the thermal rotating shallow water equations*, J. Comput. Phys., 411 (2020), p. 109414.
- [27] A. KURGANOV AND G. PETROVA, *A second-order well-balanced positivity preserving central-upwind scheme for the Saint-Venant system*, Commun. Math. Sci., 5 (2007), pp. 133–160.
- [28] R. J. LEVEQUE, *Balancing source terms and flux gradients in high-resolution Godunov methods: the quasi-steady wave-propagation algorithm*, J. Comput. Phys., 146 (1998), pp. 346–365.
- [29] X. LIU, X. CHEN, S. JIN, A. KURGANOV, AND H. YU, *Moving-water equilibria preserving partial relaxation scheme for the Saint-Venant system*, SIAM J. Sci. Comput., 42 (2020), pp. A2206–A2229.
- [30] Y. LIU, J. LU, Q. TAO, AND Y. XIA, *An oscillation-free Discontinuous Galerkin method for shallow water equations*, J. Sci. Comput., 92 (2022). Paper No. 109, 24 pp.
- [31] V. MICHEL-DANSAC, C. BERTHON, S. CLAIN, AND F. FOUCHER, *A well-balanced scheme for the shallow-water equations with topography or Manning friction*, J. Comput. Phys., 335 (2017), pp. 115–154.
- [32] S. NOELLE, Y. XING, AND C.-W. SHU, *High-order well-balanced finite volume WENO schemes for shallow water equation with moving water*, J. Comput. Phys., 226 (2007), pp. 29–58.

- [33] M. RICCHIUTO, *An explicit residual based approach for shallow water flows*, J. Comput. Phys., 280 (2015), pp. 306–344.
- [34] M. RICCHIUTO AND A. BOLLERMANN, *Stabilized residual distribution for shallow water simulations*, J. Comput. Phys., 228 (2009), pp. 1071–1115.
- [35] G. ROSATTI AND L. BEGNUDELLI, *The Riemann Problem for the one-dimensional, free-surface Shallow Water Equations with a bed step: Theoretical analysis and numerical simulations*, J. Comput. Phys., 229 (2010), pp. 760–787.
- [36] F. VILAR, *A posteriori correction of high-order discontinuous Galerkin scheme through subcell finite volume formulation and flux reconstruction*, J. Comput. Phys., 387 (2019), pp. 245–279.
- [37] Y. XING, *Exactly well-balanced discontinuous Galerkin methods for the shallow water equations with moving water equilibrium*, J. Comput. Phys., 257 (2014), pp. 536–553.
- [38] Y. XING AND C.-W. SHU, *A survey of high order schemes for the shallow water equations*, J. Math. Study, 47 (2014), pp. 221–249.